Ab Initio Study of $AgGaSe_2$ Chalcopyrite Under Extreme Conditions

12 de Marzo de 2019

Trabajo Final de Máster

ULL
Máster Universitario en Astrofísica

Autor:
Sergio Rodríguez Peña

Tutores:
Dr. Alfonso Muñoz González
Dra. Plácida Rodríguez Hernández

Index:

1 Resumen (Español)

En este trabajo se ha realizado un estudio de las propiedades estructurales, elásticas y vibracionales del $AgGaSe_2$, cuya estructura pertenece a la familia de las calcopiritas, y de su evolución con la presión. Se utilizan cálculos computacionales basados en primeros principios (*Ab Initio*) que permiten obtener de forma precisa simulaciones de las propiedades que experimentalmente serían costosas de estudiar o difícilmente accesibles en los laboratorios. Este tipo de herramientas permiten estudiar el comportamiento de los materiales cuando se someten a condiciones extremas de presión y temperatura que se dan, por ejemplo, en el interior de La Tierra. La estructura y propiedades dinámicas de un cristal determinan una amplia variedad de comportamientos, tanto micro como macroscópicos: difracción, constantes elásticas, absorción, scattering... Se utilizará el software *Vienna Ab-Initio Simulation Package* (VASP) [1] para la realización de los cálculos teóricos a partir de las posiciones atómicas obtenidas de la literatura.

Se comenzará este trabajo explicando brevemente en la Sección 3 la estructura del material estudiado: $AgGaSe_2$, explicando qué es lo que diferencia a las calcopiritas del resto de compuestos y por qué la configuración atómica de este tipo de compuestos les confiere unas ciertas características únicas. Se buscará en la bibliografía las posibles aplicaciones en las que las calcopiritas, gracias a su amplia variedad de interesantes propiedades, pueden ser utilizadas y cómo, en las últimas décadas, se han realizado diversas investigaciones, tanto experimentaales como teóricas, sobre dichas propiedades.

Posteriormente, en la Sección 4, se dará una breve explicación de la base teórica en la que se basan los cálculos realizados. El objetivo principal de las simulaciones por ordenador es la resolución de la ecuación de Schrödinger mediante métodos Ab Initio para obtener las propiedades de diversos materiales. Uno de los métodos más utilizados, y que se usará en este trabajo, es la teoría del funcional de la densidad: DFT (*Density Functional Theory*). Este método utiliza las densidades electrónicas de los múltiples átomos que conforman el material y resuelve el sistema de ecuaciones formado por las múltiples ecuaciones de Schrödinger: ecuaciones de Kohn-Sham.

Para facilitar la resolución de las ecuaciones, la DFT utiliza diferentes aproximaciones para la energía de canje y correlación. La aproximación por defecto de *VASP* es la LDA (*Local Density Approximation*), donde el funcional de la energía únicamente depende de los valores de la densidad electrónica, y no de sus derivadas. Además de la LDA, existe una gran variedad de aproximaciones, algo más complejas, que incluyen términos que dependen de la derivada de la densidad: las denominadas GGAs (*Generalized Gradient Approximations*). En este trabajo se utilizará tanto la aproximación LDA, como las GGAs de PBE (Perdew-Burke-Ernzeerhof) y su revisado para sólidos PBEsol [2].

Siguiendo con la parte de resultados, en la Sección 5 se obtendrán los parámetros de red del compuesto: a y c de la celda unidad (debido a que en condiciones normales, la estructura más estable es la tetragonal: $a = b$) y el parámetro u característico de las calcopiritas; así como el módulo de bulk (B_0) y su derivada (B_0'). Ajustando el comportamiento de los parámetros de red, en función de la presión, por mínimos cuadrados, se obtendrán las compresibilidades lineales en la red (κ_a y κ_c) en función de la presión además de la ecuación que gobierna el comportamiento de u con la presión.

Después, usando la celda primitiva para reducir el coste temporal de cálculo, se obtendrán las 6 constantes elásticas que caracterizan a las estructuras tetragonales (C_{11}, C_{12}, C_{13}, C_{33}, C_{44} y C_{66}) a presión cero, así como su evolución con la presión, y se comparará el resultado que se obtiene para B_0 del ajuste de la ecuación de estado de la energía frente al volumen con el valor procedente de las constantes elásticas. Se analizará la variación de estas constantes con la presión, hasta los 12 GPa aproximadamente. Se observará que una determinada constante elástica (C_{44}) se vuelve negativa en torno a los 2 GPa, lo que es indicativo de que a esa presión se podría producir una transición de fase. Los valores obtenidos se compararán con diversos cálculos teóricos, realizados mediante diferentes approximaciones, y con resultados experimentales. Se estudirán también las condiciones de estabilidad y se determinará que la estructura es mecánicamente inestable a presiones superiores a los 3 GPa approxidamente.

Para finalizar, con la ayuda del software PHONOPY [3], se obtendrán los fonones del sistema y la evolución de su frecuencia con el aumento de la presión en el punto Γ de la primera zona de Brillouin hasta la misma presión que en el caso de las constantes elásticas ($\approx 12\ GPa$). Estos cálculos son de gran importancia ya que ciertas transiciones de fase pueden asociarse al ablandamiento de los modos de frecuencias bajas. Veremos que uno de los modos de los fonones se ablanda sobre los 3 GPa indicando que la estructura es dinámicamente inestable (al igual que lo era mecánicamente sobre la misma presión por la constante elástics C_{44}). Se realizará un estudio de las curvas de dispersión siguiendo el camino Γ-X-P-N-Γ-M de los puntos de la primera zona de Brillouin hasta una presión de 3 GPa; además obtendremos las densidades de estados de los fonones (tanto parciales como totales) y podremos analizar qué átomos tienen una mayor contribución en los diferentes modos. Se utilizará una supercelda 2x2x2 para esta última parte y, debido al gran tiempo de cálculo requerido por el software, se limitará su obtención a la aproximación PBEsol.

Para no sobrecargar el trabajo con un gran número de gráficas, se representarán sólo los resultados obtenidos con la aproximación PBEsol (a excepción de las curvas de energía frente a volumen) ya que, como se verá posteriormente, proporciona los parametros de red más cercanos a los valores experimentales. Con esta aproximación se obtienen unos resultados intermedios comparados con las otras dos aproximaciones. Sin embargo, cuando se muestren los valores calculados en las diversas tablas, sí que se indicarán los resultados obtenidos con las tres aproximaciones.

2 Abstract

In this work we have perform a study of the structural, elastic and vibrational properties of the chalcopyrite $AgGaSe_2$ and their evolution under pressure. Computational calculations based on first principles have been used to obtain the results. They allow to obtain, in a precise way, simulations of results which experimentally would be very costly or hard to reproduce in the laboratories. This kind of tools allow the study of the behaviour of the materials when they are under extreme pressure and temperature conditions which exist, for example, in the interior of the Earth. We will use the *Vienna Ab-Initio Simulation Package* (VASP) [1] software to make the theoretical calculations using the atomic positions obtained from the literature.

To begin with, in Section 3 we will explain in a brief way the structure of the material under study: $AgGaSe_2$, explaining the importance of the chalcopyrite structure of the compounds, their possible applications and how the unique properties of this type of compounds make them different from other crystals with similar structure.

Later, in Section 4 we will make a brief explication of the theoretical base on which the calculations are based. The main goal of the computer simulation is to solve the Schrödinger equation using *Ab Initio* methods to obtain the properties of any material. One of the methods more used in the literature, and the one which we will use in this work, is the Density Functional Theory (DFT). This method uses the electronic densities of all the atoms which form the material and it solves the equation system formed with all the Schrödinger equations: Kohn-Sham equations. DFT can use multiple approximations for the exchange-correlation energy to solve the problem: the denominated GGAs (Generalized Gradient Approximations). The default approximation of the VASP software is the LDA (Local Density Approximation), where the energy functional only depends on the values of the electronic density, and not in their derivatives. In this work, we will use both the LDA approximation and the GGAs PBE (Perdew-Burke-Ernzeerhof) and its revised form for solids PBEsol [2].

In Section 5, the structural parameters of the unit cell of the compound will be obtained: a and c; as well as the Bulk modulus (B_0) and its derivative (B_0'). Adjusting by least squares we will obtain the linear compressibilities of the unit cell parameters (κ_a, κ_c) and the equation of evolution of u when increasing pressure. Afterwards, we will calculate the elastic constants up to 12 GPa and we will compare the value of B_0 obtained from the fit of the energy-volume curve with the value given by the elastic constants and with the experimental values to check the validity of the calculations. We will observe that the elastic constant C_{44} suffers a softening around 3 GPa which could indicate a phase transition from the tetragonal structure stable at atmospheric conditions. The study of the Generalized Born stability conditions will confirm that the system becomes mechanically unstable around 3 GPa.

Thanks to the PHONOPY software [3] and employing the data for the optimized cells, we will calculate the phonons of the system and their frequency behaviour under pressure at the Γ-point of the first Brillouin zone. The dispersion curves inside this zone will be obtained too, as well as the phonon density of states (both partial and total). We will show that the system is not only mechanically unstable above 3 GPa, it is also dynamically unstable. A 2x2x2 supercell will be used for these calculations. Due to the large amount of time needed by the software, this part of the work will be done using the PBEsol approximation only.

The figures shown in this work will correspond to the results obtained with the PBEsol approximation (except from the energy-volume curves) since it gives intermediate results between the three approximations and the more similar ones to the experimental results.

3 Introduction

The compound $AgGaSe_2$ belongs to the ternary chalcopyrite family (I-III-VI_2: I = Ag, Cu; III = Ga, In, Al; VI = S, Se, Te) and shows the crystalline structure corresponding to the tetragonal spatial group $I\bar{4}2d$ with four formula per unit cell. This kind of compound are isoelectronic with respect to the zinc-blend structure II-VI. An ideal chalcopyrite would correspond to a zinc-blend supercell formed by two unit cells in the c-direction; but in real chalcopyrites, the introduction of two different atoms replacing the divalent atom in the zinc-blend, one monovalent and one trivalent, induces a distortion in the tetragonal structure ($c/2a \neq 1$), resulting on a compression of the c-axis, due to the different electronegativities, and the displacement of the Se-atoms from their ideal positions by a characteristic parameter u ($u \neq 0.25$). This displacement of the Se-atoms makes that the distance between the Se and Ag-atoms were different than the Se-Ga distance (See Fig.1). All of the peculiarities of chalcopyrite compounds arise from the relative ordering of the two bounds between the incorporated atoms.

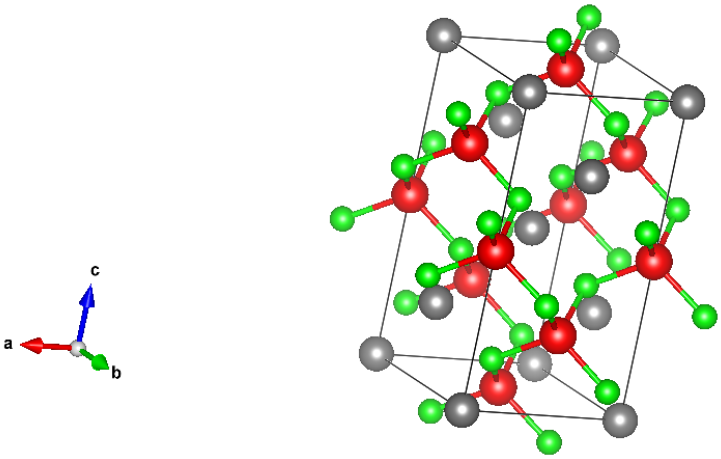

Figure 1: Unit cell of $AgGaSe_2$: Ag in grey, Ga in red and Se in green.

Although some electronic and vibrational properties of chalcopyrite compounds show similarities with their cubic homologous, fact that has been used to study these structures [4], there exist an anomalous behaviour of the band gap between the chalcopyrites and their zinc-blend analogous [5]. In $AgGaSe_2$, the band gap increases with temperature until reaching a maximum around 70 K and then it decreases from 110 K [6], linearly in both parts.

$AgGaSe_2$ presents a direct gap between the valence and conduction bands at the Γ-point and this gap, as well as in all these compounds, increases with pressure.

Chalcopyrites have a lot of practical applications, from their use in photovoltaic plates due to their semiconductor character, to their application in non-linear optics thanks to the

birefringence they show or their use in laser as doubling frequency crystals. Contrary to the chalcopyrite compounds in which Ag is substituted by Cu, Ag-chalcopyrites show a negative thermal expansion coefficient for the c-axis [7].

Classic photovoltaic plates show a great deficiency when one refers to the ability of transforming solar light into electricity. Although the theory of the photovoltaic effect is well known, the problem arises when we refer to the efficiency of the plates. The combination of various compounds allows the plates to increase their efficiency by absorbing photons which would be wasted [8], [9], [10]. The great flexibility, low cost and low weight makes the chalcopyrites a good alternative to solar cells based on Si. Besides, the combination of various materials on a multipanel cell could improve the efficiency of such solar panel up to 40% [11]. Due to its narrow gap, $AgGaSe_2$ is a great candidate to infrared detectors as well as it has shown others interesting detector properties, such as room-temperature radiation detector [12].

Chalcopyrites have a great application in laser physics too. They are a great candidate to build IR oscillators [13] thanks to their large transparency region and non-linear properties [14]. Their anisotropy allows them to be useful at frequency conversion [15], specially in IR region with CO_2 lasers [16], being even able to generate the fourth harmonic [17]. The third harmonic can also be generated and, with the inclusion of some In in the formula, it can be construct so that it is 90^o phase-matched as Takaoka & Kato discover [18]. This way, we can expand the range of frequencies in which the IR-lasers usually work. The introduction of some In in the formula allows to vary the band gap [19] and to increase the efficiency of the second harmonic generator [20].

4 Theoretical Introduction

4.1 Density Functional Theory

To obtain the physical properties of the system, we need to solve the Schrödinger equation of the crystal, minimizing the energy in relation with the electronic and nuclei positions [21]. The Hamiltonian of the system is the sum of the contributions of all the elements of the system:

$$\hat{H} = -\sum_I \frac{\hbar^2}{2M_I}\nabla_I^2 - \frac{\hbar^2}{2m_e}\sum_i \nabla_i^2 + \frac{1}{2}\sum_{I,J(I\neq J)} \frac{Z_I Z_J e^2}{\mid \mathbf{R}_I - \mathbf{R}_J \mid} + \frac{1}{2}\sum_{i,j(i\neq j)} \frac{e^2}{\mid \mathbf{r}_i - \mathbf{r}_j \mid} - \sum_{i,I} \frac{Z_I e^2}{\mid \mathbf{R}_I - \mathbf{r}_i \mid} \tag{1}$$

where $\mathbf{R}_I$ and $\mathbf{r}_i$ are the nuclei and electronic positions respectively, M_I and m_e their masses, Z_I the I-nuclei charge and e the electron charge.

Once defined the Hamiltonian, the time-dependent Schrödinger equation:

$$\hat{H}\Psi(\mathbf{R}_I;\mathbf{r}_i) = E\Psi(\mathbf{R}_I;\mathbf{r}_i) \tag{2}$$

where $\Psi(\mathbf{R}_I;\mathbf{r}_i)$ is the wave function of the system and E the energy, allows us to obtain all the properties of the system under study. Due to the great difficulty in resolving this problem, it is common, and advisable, to use some approximations that simplify the problem and that keep their ab initio character. Thus, ab initio calculations are very precise, but, as almost anything in physics, they need some approximations.

The main approximation is the adiabatic or Born-Oppenheimer one. It is based on the fact that the electrons are much lighter than the atomic nuclei and, as the electric forces between them are of the same order, the velocity of the electrons is much higher than that of the nuclei. This means that one is able to treat the problem splitting the movement of the nucleus from the electrons and to suppose that the electrons are affected by a static potential generated by the static nuclei.

Density Functional Theory (DFT) is the most used approximation to obtain the ground state of the electrons using first principles. It is used to describe the multielectronic system under the action of an external potential (V_{ext}), and the Hamiltonian is:

$$\hat{H} = -\frac{\hbar^2}{2m_e}\sum_i \nabla_i^2 + \sum_i V_{ext}(\mathbf{r}_i) + \frac{1}{2}\sum_{i,j(i\neq j)} \frac{e^2}{\mid \mathbf{r}_i - \mathbf{r}_j \mid} \tag{3}$$

This theory was formulated by Hohenberg & Kohn [22] and it is based on two theorems:

1. For any particle system interacting with an external potential $V_{ext}(\mathbf{r})$, the potential is determined exclusively by the particle density on the ground state $n_0(\mathbf{r})$ and, therefore, as $\hat{H}$ is determined by $V_{ext}(\mathbf{r})$, the system properties are determined by $n_0(\mathbf{r})$.

2. For any $V_{ext}(\mathbf{r})$, the energy is an unique functional ($E[n]$) of the particle density $n(\mathbf{r})$. Minimizing this functional with respect to the variations of $n(\mathbf{r})$ will allow us to obtain the energy and density of the ground state.

This functional can be expressed as:

$$E[n] = \int V_{ext}(\mathbf{r})n(\mathbf{r})d\mathbf{r} + F[n] \tag{4}$$

where $F[n]$ is an independent functional of the external potential (atomic units are used). It has to satisfy that $\int n(\mathbf{r})d\mathbf{r} = N$ (where N is the total number of electrons on the system).

When the system is formed by N non-interacting electrons in the presence of an external potential, Kohn & Sham [23] found out that the functional $F[n]$ is just the functional of the kinetic energy $T_s[n]$. Then, following this approach, an interacting system has an energy:

$$E[n] = \int V_{ext}(\mathbf{r})n(\mathbf{r})d\mathbf{r} + \frac{1}{2}\int \frac{n(\mathbf{r})n(\mathbf{r}')}{\mid \mathbf{r} - \mathbf{r}' \mid} d\mathbf{r}d\mathbf{r}' + T_s[n] + E_{xc}[n] \tag{5}$$

where $E_{xc}[n]$ is the exchange correlation energy and the second term correspond to the Hartree energy.

Solving self-consistently the set of Schrödinger equations for one particle,

$$\left\{-\frac{1}{2}\nabla^2 + V_{eff}(\mathbf{r})\right\}\psi_i(\mathbf{r}) = \varepsilon_i\psi_i(\mathbf{r}) \quad ; \quad i = 1...N \tag{6}$$

which correspond to the Kohn-Sham equations, the ground state density of the system formed by N interacting electrons can be obtained. This density is given by $n(\mathbf{r}) = \sum_{i=1}^{N} \mid \psi_i(\mathbf{r}) \mid^2$. The effective potential for an electron system in the ion external potential is:

$$V_{eff}(\mathbf{r}) = V_{ext}(\mathbf{r}) + \frac{1}{2}\int \frac{n(\mathbf{r})}{\mid \mathbf{r} - \mathbf{r}' \mid} d\mathbf{r}' + \mu_{xc}(n(\mathbf{r})) \tag{7}$$

being

$$\mu_{xc}(n(\mathbf{r})) = \frac{\partial E_{xc}[n(\mathbf{r})]}{\partial n(\mathbf{r})} \tag{8}$$

However, the exact form for the exchange correlation functional is unknown. It is necessary to make approximations and to suppose an exchange correlation energy which can be a local or quasi-local functional. The LDA approximation supposes that the exchange correlation energy is the same at any point that the density of an homogeneous electron gas $\varepsilon(n(\mathbf{r}))$. LDA approximates the energy functional as:

$$E_{xc}[n] = \int n(\mathbf{r})\varepsilon(n(\mathbf{r}))d\mathbf{r} \tag{9}$$

When the density $n(\mathbf{r})$ varies slowly, LDA obtains great results and is one of the approximations most used in the literature.

It exists different approximations for $E_{xc}[n]$ that improve the final results given by the LDA approximation when we treat with solids or molecules. This kind of approximations include a density gradient, from there their name: Generalized Gradient Approximations (GGAs). In general, LDA overestimates the cohesion energy and the GGAs underestimates it.

To solve the one-particle Kohn-Sham equations in an external effective potential, the wave functions are expanded in different bases. Typically there are three basic approximations that can be applied:

- Plane waves basis set: to use plane waves, we require Fourier transformations between the real and reciprocal spaces. It is easy to use with *Ab Initio* methods, but a great number of plane waves are needed to obtain the potentials and the wave functions correctly.
- Localized atomic-like orbitals (LCAOs): it requires a lower number of orbitals for each atom but it is difficult to get a good convergence.
- Atomic spheres methods: close to the nuclei, magnitudes behave similarly to atomic ones, and in the interatomic regions, those magnitudes vary slowly. This method combines both the advantages of the plane waves and the localised functions, but it is difficult to implement.

The wave function has oscillations as it approaches the nucleus of an atom and the Coulombic potential has a singular point when r tends to 0. However, since the scattering theory states that the properties of the valence electrons are only affected by the external part of the potential, we can use a pseudopotential and a pseudo-wavefunction function which set a cutting radius. Outside this radius, both the pseudopotential and the pseudo-wavefunction are similar to the real ones; but in the internal region, the pseudopotential lacks of the singularity at $r = 0$ and the pseudo-wavefunction does not have the oscillations (See Fig.2).

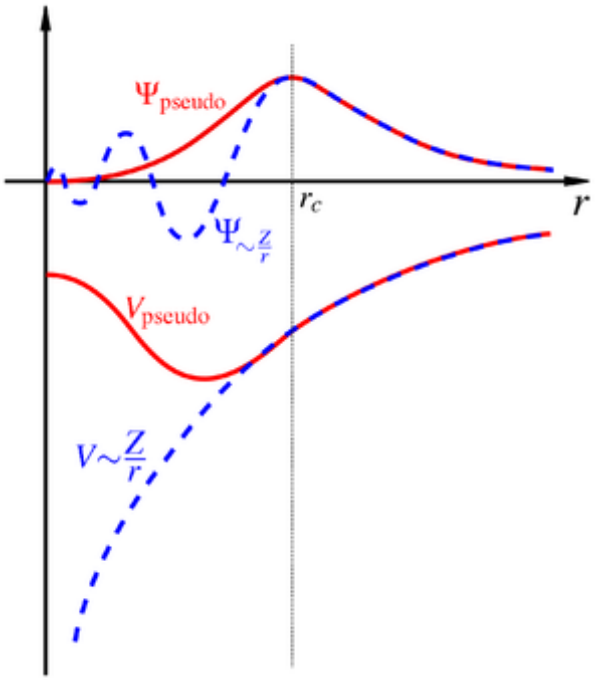

Figure 2: Representation of the pseudopotential and pseudo-wavefunction with respect to the real ones [24].

In the case of crystals, the potential in which the electrons are immerse is periodic due to the positions of the nuclei. Crystals are formed by the repetition, in the three spatial directions, of the unit cell. This periodicity really simplifies the Kohn-Sham equations. It can be applied the Bloch theorem to the wave functions and they can be written as the product of a plane wave and a function with the same periodicity of the crystal.

Using the periodicity of the crystal, each electronic wave function can be expressed as sum of plane waves:

$$\psi_{n,\mathbf{k}}(\mathbf{r}) = \sum_{\mathbf{G}} C_{n,\mathbf{k}+\mathbf{G}} e^{i(\mathbf{k}+\mathbf{G})\cdot\mathbf{r}} \tag{10}$$

where the sum runs over the reciprocal lattice vectors $\mathbf{G}$, n is the band number and $\mathbf{k}$ is a vector of the Brillouin zone. It is necessary to take into account all the $\mathbf{k}$-points of the filled states to get the correct state density, but the electronic wave functions in close $\mathbf{k}$-points are nearly identical. The most popular method to get an accurate result in the Brillouin zone using a small number of $\mathbf{k}$-points is the Monkhorst-Pack scheme [25].

The plane wave basis set in which the wave functions are expanded must be, at first, infinite. However, in practise, plane waves with small kinetic energy have a more important $C_{n,\mathbf{k}+\mathbf{G}}$-coefficient. We can truncate the plane waves set at a maximum energy E_{cutoff} and to eliminate the plane waves with greater energies. This E_{cutoff} is:

$$\frac{\hbar^2}{2m_e} \mid \mathbf{k}+\mathbf{G} \mid^2 < E_{cutoff} \tag{11}$$

As E_{cutoff} increases, the error when calculating the total energy becomes smaller. Its value must be chosen so that the system properties would have correctly converged.

From here, the quantities in which we are interested can be obtained by solving the Kohn-Sham equations in a self-consistent way. The pseudopotential V_{ext}^{pseudo} is obtained from the atomic positions of the system and this leads to a first electronic charge density $n^{in}(\mathbf{r})$. With this density we get a new effective potential and, solving again the Kohn-Sham equations, a new density $n^{out}(\mathbf{r})$. One can repeat this process until the potentials and the densities converge. To be sure that the system has converged in a relaxed geometry, the forces over the atoms must be close to zero. Those forces are calculated using the Hellman-Feynman theorem.

4.2 Elastic Constants

Elastic constants characterise the behaviour of a system when it is submitted to an external strain. They are defined as the second derivative of the energy with respect to the strain tensor per unit volume. They are given by the relation:

$$C_{ijkl} = \frac{\sigma_{ij}}{\epsilon_{kl}} \tag{12}$$

where ϵ_{kl} and σ_{ij} are the strain and stress tensor components respectively. By symmetry, the elements of C_{ijkl} can be reduced to a 6x6 matrix C_{ij} and its number of components depends on the symmetry of the system [26].

To calculate the elastic constants of a system, the unit cell is slightly deformed changing the Bravais lattice vectors from $\mathbf{R} = (\mathbf{a}, \mathbf{b}, \mathbf{c})$ to $\mathbf{R}' = (\mathbf{a}', \mathbf{b}', \mathbf{c}')$ using the tension matrix:

$$\mathbf{R}' = \mathbf{R} \begin{pmatrix} 1+e_{xx} & \frac{1}{2}e_{xy} & \frac{1}{2}e_{xz} \\ \frac{1}{2}e_{xy} & 1+e_{yy} & \frac{1}{2}e_{yz} \\ \frac{1}{2}e_{zx} & \frac{1}{2}e_{yz} & 1+e_{zz} \end{pmatrix} \tag{13}$$

The crystal's deformation induces a change in the total energy of the system given by:

$$U = \frac{E_{tot} - E_0}{V_0} = \frac{1}{2}\sum_{i=1}^{6}\sum_{j=1}^{6} C_{ij} e_i e_j \tag{14}$$

where E_0 is the non-deformed system energy. This definition of the energy allows to define the stability criteria to know if a determined structure is stable or not. A lattice is dynamically stable if U is positive for any small deformation. This fact imposes some restrictions on the possible values of the elastic constants C_{ij}: the Born stability criteria [27].

Depending on the crystal structure, the symmetry of the lattice reduces the number of the independent elastic constants and thus the stability relations change in terms of the symmetry [28]. Beside, the relations change when pressure is taken into account too. When we will obtain the elastic constants for the range of pressures under study, we will also study five stability criteria for the tetragonal structure. In this case, the relations of stability used are the generalized Born stability criteria. For a tetragonal crystal under hydrostatic pressure, these generalized criteria are:

$$\begin{gathered} C_{11} - P > 0 \quad ; \quad C_{44} - P > 0 \quad ; \quad C_{66} - P > 0 \\ C_{11} - C_{12} - 2P > 0 \quad ; \quad (C_{33} - P)(C_{11} + C_{12}) - 2(C_{13} + P)^2 > 0 \end{gathered} \tag{15}$$

The violation of one or more stability criteria indicate that the structure under study is mechanically unstable.

Another important fact related with the elastic constants is that they allow us to obtain the bulk modulus of the system. We can use two approximations to obtain it: the Voigt [29] and the Reuss [30] approximations.

$$B_V = \frac{1}{9}(2(C_{11} + C_{12}) + C_{33} + 4C_{13}) \tag{16}$$

$$B_R = \frac{(C_{11} + C_{12}C_{33} - 2C_{13}^2}{C_{11} + C_{12} + 2C_{33} - 4C_{13}} \tag{17}$$

as well as others structural factors like compressibility factors, shear modulus, Young modulus or Poisson ratio [31]. They are also related to the linear compressibilities of the lattice parameters. For the tetragonal structure under study, the linear compressibilities are given by:

$$\kappa_a = \frac{C_{33} - C_{13}}{C_{33}(C_{11} + C_{12}) - 2C_{13}^2} \tag{18}$$

$$\kappa_c = \frac{C_{11} + C_{12} - 2C_{13}}{C_{33}(C_{11} + C_{12}) - 2C_{13}^2} \tag{19}$$

In Section 5 we will compare the results given for the linear compressibilities κ_a and κ_c obtained from the fit of a and c against pressure and the ones given by the elastic constants as a method of testing that the results are correct.

4.3 Phonons

The vibrations induced on a crystal by moving the atoms from their equilibrium positions are denominated phonons. At being displaced, the atoms suffer a recovering force that makes them to vibrate at a certain characteristic frequencies. These vibrations determine a great variety of physical properties of materials and, in some cases, they can be related with phase transformations, specially the lower frequency modes. The appearance of an imaginary frequency mode could indicate that the structure is dynamically unstable.

Considering an infinite periodic crystalline material with N unit cells and n atoms per cell, we define the displacements of the j-atom in the L-lattice vector cell as:

$$\mathbf{u}_{jL} = \mathbf{r}_{jL} - \mathbf{r}_{0,jL} \tag{20}$$

where $\mathbf{r}_{0,jL}$ is the equilibrium position of the j-atom in the L-lattice vector cell. The static energy of the crystal E is expanded on a Taylor series using these displacements:

$$E = E_0 + \frac{1}{2} \sum_{jj'LL'} \mathbf{u}_{jL}^T \mathbf{D}_{jLj'L'} \mathbf{u}_{j'L'} + ... \tag{21}$$

where E_0 is the zero pressure static energy and $\mathbf{D}_{jLj'L'}$ the second derivative 3x3 matrix of the energy with respect to the displacements:

$$(\mathbf{D}_{jLj'L'})_{\alpha\beta} = \frac{\partial^2 E}{\partial(\mathbf{u}_{jL})_\alpha \partial(\mathbf{u}_{j'L'})_\beta} \tag{22}$$

where α and β correspond to the Cartesian coordinates (x, y and z). Notice that there is no linear term because the static energy is minimum at equilibrium.

Making use of the harmonic approximation, we suppose that the atoms vibrate inside an harmonic well around the equilibrium position and that these vibrations are small compared to the interatomic distances. With this approximation, the Taylor expansion series is truncated at second order and the movement equation for each atom sets as:

$$m_j \ddot{\mathbf{u}}_{jL} = \mathbf{F}_{jL} = \sum_{j'L'} \mathbf{D}_{jLj'L'} \mathbf{u}_{j'L'} \tag{23}$$

where m_j is the j-atom mass and $\mathbf{F}_{jL}$ the force over the atom at position jL. There exist one equation for each Cartesian coordinate for each atom ($3nN$ equations in total) and each of them have one solution for the displacement in terms of planes waves:

$$\mathbf{u}_{jL} = \epsilon_{\mathbf{k}\nu j} e^{i(\mathbf{k}\cdot\mathbf{L} - \omega_{\mathbf{k}\nu} t)} \tag{24}$$

The displacement vector ($\epsilon_{\mathbf{k}\nu j}$) gives the propagation direction of the atomic displacements wave and $\mathbf{k}$ represents the vectors of the first Brillouin zone. ν is the index that runs over the possible solutions of $\mathbf{k}$ and goes from 1 to $3n$. The atomic displacements wave (or its linear combinations) is what is known as a phonon.

Substituting on the movement equation (Eq.23):

$$m_j \omega_{\mathbf{k}\nu}^2 \epsilon_{\mathbf{k}\nu j} = \sum_{j'} \left(\sum_{L'} \mathbf{D}_{j0j'L'} e^{i\mathbf{k}\cdot\mathbf{L'}} \right) \epsilon_{\mathbf{k}\nu j'} \tag{25}$$

with $\mathbf{L} = 0$ referring to the reference unit cell. Defining $\eta_{\mathbf{k}\nu j}$ as:

$$\epsilon_{\mathbf{k}\nu j} = \frac{1}{\sqrt{m_j}} \eta_{\mathbf{k}\nu j} \tag{26}$$

it allows us to define the matrix between brackets in Eq.(25) as:

$$\mathbf{D}_{jj'}(\mathbf{k}) = \frac{1}{\sqrt{m_j m_{j'}}} \sum_{L'} \mathbf{D}_{j0j'L'} e^{i\mathbf{k}\cdot\mathbf{L}'} \tag{27}$$

This way, this equation becomes:

$$\omega^2_{\mathbf{k}\nu} \eta_{\mathbf{k}\nu j} = \sum_{j'} \mathbf{D}_{jj'}(\mathbf{k}) \eta_{\mathbf{k}\nu j'} \tag{28}$$

where $\mathbf{D}(\mathbf{k})$ is the dynamical matrix (the collection of all the 3x3 n matrices in one $3n$x$3n$ squared matrix). Transforming the dynamical matrix to the real space we get the constant force matrix $\mathbf{C}(\mathbf{L})_{j\alpha j'\beta}$:

$$\mathbf{C}(\mathbf{L})_{j\alpha j'\beta} = \frac{1}{\sqrt{m_j m_{j'}}} \frac{\partial^2 E}{\partial(\mathbf{u}_{j0})_\alpha \partial(\mathbf{u}_{j'L'})_\beta} \tag{29}$$

Joining all the atomic displacements in the displacement vector $\eta_{\mathbf{k}\nu}$, one can put all the equations in one unique eigenvalues equation:

$$\omega^2_{\mathbf{k}\nu} \eta_{\mathbf{k}\nu} = \mathbf{D}(\mathbf{k}) \eta_{\mathbf{k}\nu} \tag{30}$$

where diagonalizing the dynamical matrix allows us to get the frequencies and the eigenvectors of the phonons ($\omega_{\mathbf{k}\nu}$ and $\eta_{\mathbf{k}\nu}$ respectively). Eigenvectors are also known as the normal modes or polarisation vectors. As the dynamical matrix is Hermitian ($\mathbf{D}_{ij} = \mathbf{D}^*_{ij}$), the squares of the frequencies are real numbers and the eigenvectors of the phonons can be chosen as an orthonormal set.

Using the previous theory, there exist two main Ab Initio methods to calculate the frequency of the phonons: the frozen phonons method and the density functional perturbation theory (DFPT) [32]. The method that we will use on this work will be the first one [3], despite the fact that DFPT does not need the use of supercells. DFPT is based on the calculation of the frequencies from the response of the system using perturbation theory.

The frozen phonons method calculates the frequencies from the energy differences or the forces that appear on the atoms when they are slightly displaced from their equilibrium positions a distance u. By making series of small displacements and calculating the total energy and forces over the atoms, using the Hellman-Feynman theory, the interatomic force constants and the dynamical matrix of the system are obtained. As mentioned before, diagonalizing the dynamical matrix, one can get the frequency of the phonons. The displacement of the atoms needs to be small enough so that the harmonic approximation were still valid, but no too small for the energy change to be insignificant. The main problem of the frozen phonons method is that it only allows to make calculations easily at the Γ-point ($\mathbf{k}$=0). To be able to get results in other points, this method needs the use of supercells.

In our study, we will not include the study of the LO-TO splitting (it is possible to include it using the Born effective charges and the dielectric constant in order to take into account the effect of the electric field).

5 Results and Discussion

5.1 Overview of the simulation

Before starting the discussion of the results obtained in this work, it is important to shortly remember all the aspects of the following simulations. The energy was obtained making use of the Density Functional Theory (DFT) implemented in the Vienna Ab-initio Simulation Package (VASP). The pseudo potentials were employed with the Projector Augmented Wave scheme (PAW) [33]. The energy-volume curves, lattice parameters, linear compressibilities and elastic constants were calculated using the Local Density Approximation(LDA) and, from the great variety of Generalized Gradient Approximations (GGAs), the Perdew-Burke-Ernzeerhof (PBE) approximation and its revised form for solids (PBEsol). In the case of phonons, due to the very large time required by the computational calculations, we only use the PBEsol approximation since it is the approximation which gives the better structural results.

The energy cutoff for the planewave basis was set in 400 eV and it was kept in this value for all the following calculations. To consider that the structure is relaxed (optimized configuration) difference between two consecutive steps was set in 10^{-6} eV for the energy and to 0.004 $eV/$Å for the forces on the atoms. The maximum number of ionic steps was 100 for the structural calculations. The integration on the Brillouin zone was performed with a grid of 30x30x30 k-special points obtained with the Monkhorst-Pack scheme [25]. For the calculation of the elastic constants a grid of 6x6x6 kpoints was used with only one ionic step, since we do not have to let the structure to relax if we want to calculate the elastic constants. The elastic tensor is determined by performing six distortions of the lattice and deriving the elastic constants from the strain-stress relationship [34]. For the calculation of the phonons, the convergence achieved in energy was 10^{-7} eV to improve the accuracy of the results and we use 30 kpoints. These convergence parameters were used after performing very careful convergence tests.

5.2 Structural Parameters

Thanks to the data provided by the literature, using the lattice vectors and the atomic positions in the unit cell, we were able to simulate the structure at different pressures and volumes to study the behaviour of the compound and to obtain the relaxed state at 0 GPa. We have simulated the structure till a pressure of 12 GPa (approximately) in all three approximations (LDA, PBE and PBEsol). To observe correctly the minimum in the energy-volume curve, negative pressures have been simulated too. The points calculated are fitted with the Murnaghan equation of state [35] to obtain the relaxed volume (V_0), the bulk modulus (B_0) and its first derivative (B_0').

We can see in Fig.3 a bigger concentration of calculated points around the minimum of each curve to get a better adjustment at the minimum. We see that the energy range in which the minimum is localised is quite similar for the PBE and PBEsol approximations, while the LDA gives a more negative result. We can observe that the parabolic behaviour is only valid

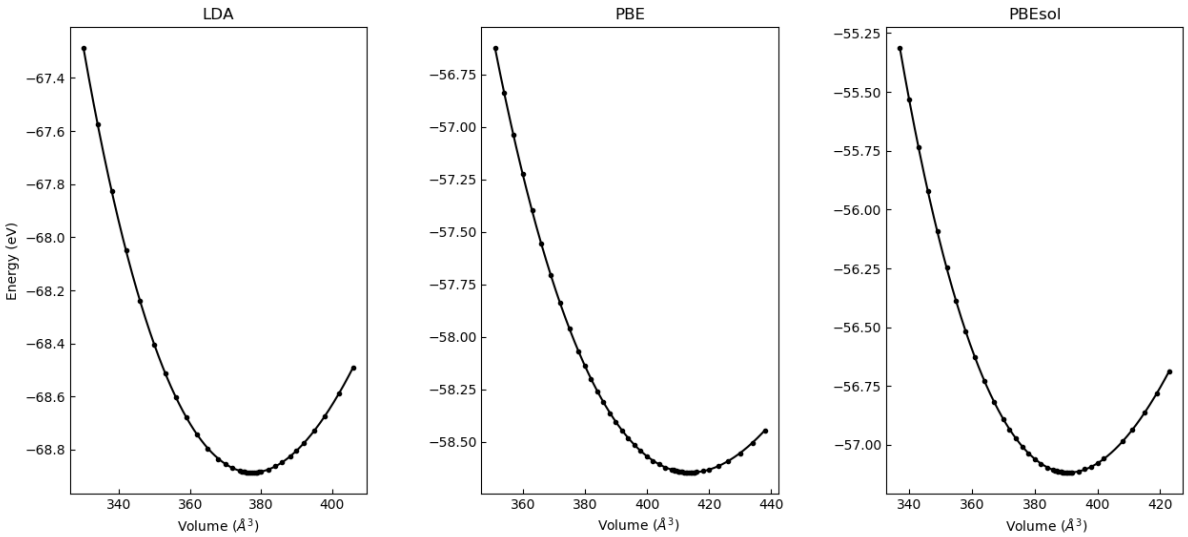

Figure 3: Energy of the system versus the volume of the unit cell in the three approximations for the exchange-correlation energy (LDA, PBE and PBEsol). Points represent the values calculated and the solid line the adjustment.

near the minimum, where the curves have a very parabolic form, but when we separate from the minimum, the curve is wider by the right than from the left; i.e. more energy is needed to compress the crystal than to stretch it. The values obtained for V_0, B_0 and B_0' compared with the data of others authors are shown in Tab.1.

		V_0 (Å^3)	B_0 (GPa)	B_0'
This work	LDA	377.479	67.099	4.361
	PBE	413.898	50.472	4.228
	PBEsol	390.773	59.947	4.260
Asokamani et al. [36]		390.44	59.86	-
Chahed et al. [37]		376.574	64.624	4.7017
Chen et al. [38]		411.39	50.7	5.02
Ouahrani et al. [39]		414.482	53.07	4.0076
Orlova et al. [40]		390.7	46	-

Table 1: Comparison of values of the volume (V_0), bulk modulus (B_0) and its derivative (B_0') at zero pressure.

All of the data shown in Tab.1 have been obtained theoretically using different methods, except the data of Orlova et al. [40] which were obtained by X-ray diffraction. We see that results on $AgGaSe_2$ are scarce. The theoretical methods used by the rest of the authors are: *Tight Binding Linear Muffin Tin Orbital* method within *Atomic Sphere Approximation* (TBLMTO-ASA) and LDA of Asokamani et al. [36]; *Linear Augmented Plane-Wave* plus local orbitals (L/APW+lo) of Chahed et al. [37]; Perdew and Wang GGA (PW91) of Chen et al. [38] and PBE96 of Ouahrani et al. [39]. Comparing data we observe that our PBEsol results are almost exactly the same as the results of Asokamani (in the absence of B_0') and our PBE

ones to the results of Chen, while with LDA we obtain results similar to Chahed. Ouahrani also obtains similar results that us using PBE. The volume experimentally determined by Orlova is the same as our volume with PBEsol, so we can say that in terms of lattice parameters, this approximation gives the better structural results; however, his value for B_0 is smaller than any of our approximations.

Another fact that came to mind when looking this results is that the bulk modulus varies significantly from one approximation to another, but all of them give results greater than the experimental value. One possible reason for this is that the experimental results do not have access to negative pressures. Besides, our three approximations give similar results for B_0', similar also to the ones reported by others authors. Other results found on the literature that have not been included on Tab.1 show these same characteristics. It is well known that many experimental values of B_0 are affected by the limited number of data and the assumption of a fixed value for B_0'.

One interesting fact with the I-III-VI_2 chalcopyrites is that they show a linear relation between the bulk modulus and the equilibrium volume [36], being this smaller for the bigger compounds. This authors have also found that the melting point is related with the bulk modulus, and thus with the equilibrium volume. The melting point increases with B_0 following a linear relation and it is bigger for the compounds with smaller volumes.

Studying the variation of the volume with pressure has allowed us to observe the behaviour of the structural parameters under pressure. The curves presented in the Fig.4 correspond to the PBEsol approximation. The calculation for the other two approximations were made too and they show a similar behaviour.

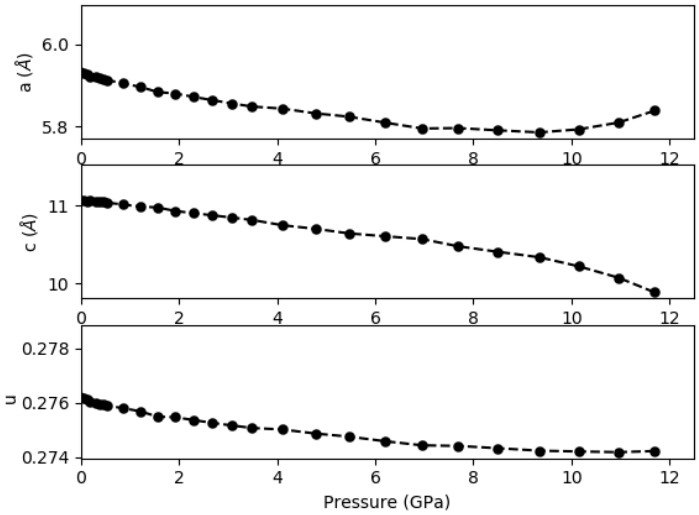

Figure 4: Evolution of the lattice parameters a and c, and the internal parameter u under pressure in the PBEsol approximation.

The behaviour of the parameters is the expected, a reduction of their values due to the pressure induced, until reaching 8 GPa. From here, a becomes nearly constant and it suddenly increases at 10 GPa. This behaviour matches with the change in the slope of c at the same

pressure. We can see that the decrease of c is much more pronounced than that of a wich, which indicates that the tetragonal distortion ($c/2a < 1$) becomes more important with pressure. This change in the evolution of a and c with increasing pressure could indicate a phase transformation. Arora et al. [41] reported in a Raman spectroscopy study that $AgGaSe_2$ actually undergoes over 3 phase transitions on the range under study in Fig.4: at 3, 5.1 and 8.3 GPa respectively. Another posterior study made by Tinoco et al. [42] reported in a X-ray absorption spectroscopy the same three transformations, but with small changes in the pressures. From the chalcopyrite structure, stable at zero pressure, $AgGaSe_2$ transforms to a mixture of two phases (the initial chalcopyrite one and an unidentified α-phase) at 2.6 GPa. Then, from 5 to 10 GPa, the structure becomes orthorhombic and finally, at 10 GPa, it undergoes another phase transformation to a tetragonal structure. Observing with more detail the Fig.4 we can see that the first transformation is inappreciable on the plots.

Although in the present work we do not study the evolution under temperature, it can be pointed out that [43],[44] while the a-axis expands with temperature, the c-axis compresses with almost the same thermal expansion coefficient.

The values for the relaxed structure at 0 GPa obtained by the simulation are compared in Tab.2 with other authors data.

		a_0 (Å)	c_0 (Å)	u_0
This work	LDA	5.849	10.989	0.2742
	PBE	6.057	11.234	0.2794
	PBEsol	5.931	11.094	0.2762
Asokamani et al.[36]		5.985	10.901	0.272
Chahed et al. [37]		5.838	11.022	0.275
Chen et al. [38]		6.0529	11.210	0.2794
Ouahrani et al. [39]		6.0579	11.2943	0.2788
Sharma et al. [45]		5.91	11.24	0.275
Lazewski and Parlinski [46]		5.916	10.879	0.276
Orlova et al. [40]		5.9915	10.8831	-

Table 2: Structural parameters of $AgGaSe_2$ at zero pressure.

It is worth noting that LDA tends to underestimate the results with respect to the other approximations when we refer to the structural parameters. This underestimation makes that the bulk modulus predicted by LDA were bigger that the PBE and PBEsol ones as it is shown in Tab.1.

Again, as in Tab.1, the only experimental values of Tab.2 are those of Orlova [40]. As many of the theoretical methods of these authors have already been mentioned in Tab.1, we will indicate only the new ones: Sharma et al. [45] use the Wu-Cohen GGA approximation and Lazewski and Parlinski [46] use a different type of approximation (Universal Force Field (UFF)) which they claim is faster and simpler, and thus more convenient for bigger structures. Comparing results, we observe that, as in Tab.1, the results of the Chahed are closer to our LDA results, and the results of Chen and Ouahrani are similar to our PBE results. This time, Asokamani do not obtain results so close to our PBEsol values. Sharma gets a a_0 close to our

PBEsol one but a c_0 value more similar to our PBE result, while Lazewski and Parlinski get values between our LDA and PBEsol results. The experimental results of Orlova et al. for c_0 is between our values for PBE and PBEsol, but the a_0 value is closer to our LDA approximation.

We can see the great variety of results, but it is also true that no author gives an extremely different result. Focusing on u_0, we see that the differences are very small between all the approximations. As can be seen, our results are in very good agreement with the experimental data, from which they differ only 1% or 2%.

5.3 Linear Compressibility

Studying the variation of the structural parameters with pressure (Fig.4), we can obtain their linear compressibilities. We have adjusted the calculated points by the least squared method and knowing that

$$\kappa_a = -\frac{1}{a}\frac{\partial a}{\partial P} \quad ; \quad \kappa_c = -\frac{1}{c}\frac{\partial c}{\partial P} \tag{31}$$

we have obtained the linear compressibilities. The results for the PBEsol approximation are shown in Fig.5.

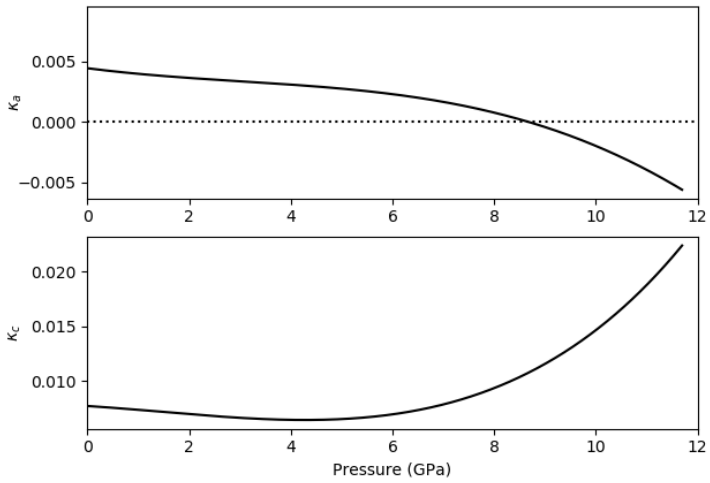

Figure 5: Linear compressibilities (in GPa^{-1}) of the lattice parameters a and c of $AgGaSe_2$ under pressure for the PBEsol approximation.

As mentioned before, the results for the LDA and PBE approximations were calculated too and the PBEsol results are approximately in the middle of these results. We observe in Fig.5 that the linear compressibility of a (κ_a) becomes negative when this parameter, a, start to increase instead of decreasing with pressure. This also happens for the other two approximations, occurring at a higher pressure (10 GPa) with LDA and at a slightly higher pressure for PBE. We observe that κ_c decreases with pressure till 4 GPa; but, as we will see later, at this pressure the chalcopyrite structure is unstable. This behaviour is also observed with the LDA and PBE approximations.

As for the variation of the internal parameter u with pressure (Fig.4), we fit it by least squared to a polynomial (Fig.6). Polynomials of different order have been proven, but the best adjustment is obtained with a third order polynomial: $u = A + BP + CP^2 + DP^3$. The values for the coefficients of the adjustment equation are shown in Tab.3.

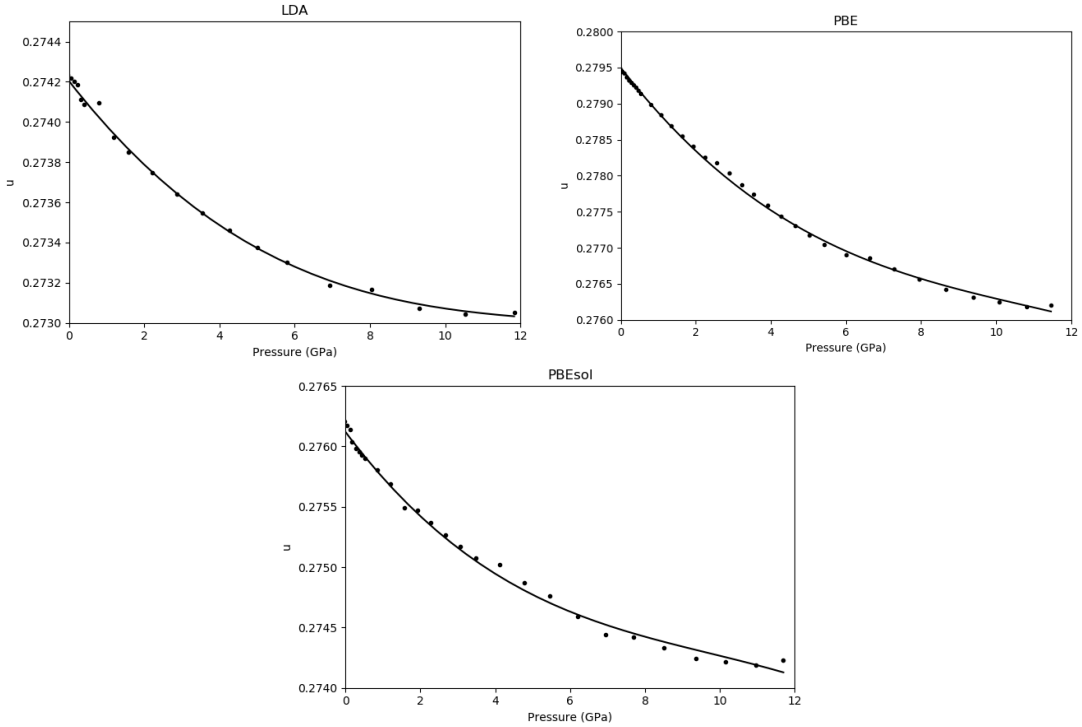

Figure 6: Adjustment of the theoretical values of u for the three approximations.

Approx.	A	B (GPa^{-1})	C (GPa^{-2})	D (GPa^{-3})
LDA	0.2742	-0.00024	0.000017	-0.0000004
PBE	0.2795	-0.00067	0.000051	-0.000002
PBEsol	0.2761	-0.00041	0.000035	-0.000001

Table 3: Values of the coefficients of the adjustment polynomial.

We observe that all three approximations have negative coefficients for the odd powers of the pressure. The D-coefficient is very small, but we have included it because the adjustment to a second order polynomial were not so good as this of third order. The errors of the coefficients are omitted, but it is worth mentioning that they increase from A to D. However, the error for D was inferior to 10%.

The values obtained for the linear compressibility can be compared with other results from the literature in Tab.4.

We observe in Tab.4 that Sharma is the only one that gets a bigger compressibility for a than for c. There is no explanation why it is this way, even when all experimental data and

		κ_a (GPa^{-1})	κ_c (GPa^{-1})
This work	LDA	0.0041	0.0066
	PBE	0.0057	0.0085
	PBEsol	0.0044	0.0077
Sharma et al. [45]		0.0062	0.0055
Lazewski et al. [47]		0.0042	0.0077
Orlova et al. [40]		0.00608	0.01007
Fouret et al. [48]		0.0047	0.00732

Table 4: Values of the linear compressibilities at zero pressure compared with other authors.

other theoretical calculations give the opposite result ($\kappa_a < \kappa_c$). Both Sharma and Lazewski obtain their results by theoretical calculation while Orlova and Fouret are experimental (X-ray diffraction [40] and inelastic neutron scattering [48] respectively). Sharma uses the Wu-Cohen GGA [45] and Lazewski a general GGA [47]. Comparing results, we see that both Fouret and Lazewski obtain results which are really close to our PBEsol ones, Orlova gets results even greater than us with the PBE approximation and the values of Sahrma are difficult to interpret: its value for κ_a is bigger than any of ours while κ_c is smaller. Our PBEsol results are in very good agreement with the experimental ones of Fouret et al.

The values in Tab.4 allow us to obtain the bulk modulus. It is defined as the inverse of the total compressibility of the crystal ($B_0 = 1/\kappa_T$), where:

$$\kappa_T = 2\kappa_a + \kappa_c \tag{32}$$

Using the linear compressibility of Tab.4, the bulk modulus obtained is: $B_0 = 67.568,\ 50.251$ and $60.606\ GPa$, respectively for the LDA, PBE and PBEsol approximations. We observe that these values are very similar to the values obtained by the fit of the energy-volume curves in Tab.1.

5.4 Elastic Constants

Due to the tetragonal structure of $AgGaSe_2$, the number of independent constants are reduced by symmetry to only six: C_{11}, C_{33}, C_{12}, C_{13}, C_{44} and C_{66}. We compare the values obtained with our simulations for the elastic constants at $0\ GPa$ with other theoretical and experimental results in Tab.5.

On a first look to the Tab.5, the first thing that comes to mind is the great variety of results that appear depending on the author and the approximation employed for the exchange-correlation energy. All the data correspond to theoretical calculations, except for the experimental ones of Fouret et al. [48] obtained via neutron scattering. This lack of experimental values for the elastic constants could be due to the difficulty of growing crystals of this compound [51]. As said before, Ouahrani et al. [39] use the PBE96 approximation and Lazewski et al. [47] a general GGA. Karki et al. [49] use the common LDA approximation and Verma et al. [50] use a different method: ionic charge theory. Comparing results of Tab.5 we observe that most of the values of the constants of Ouahrani are closer to our PBE results, except for C_{44} which is closer to LDA, and that the results of Lazewski et al. are more similar

		C_{11}	C_{33}	C_{12}	C_{13}	C_{44}	C_{66}
This work	LDA	91.009	81.765	62.543	60.290	26.584	32.410
	PBE	70.624	62.303	44.536	43.802	23.495	26.765
	PBEsol	82.318	71.330	55.645	53.049	22.714	29.162
Ouahrani et al. [39]		74.95	59.57	41.03	43.03	30.10	21.62
Lazewski et al. [47]		86.4	72.4	55.2	52.9	20.3	25.3
Karki et al. [49]		92	70	60	56	26	17
Verma et al. [50]		83.6	96.5	52.3	61.1	35.4	32.2
Fouret et al. [48]		80.1	70.7	51.6	52.6	21.2	24.7

Table 5: Values of the elastic constants (in GPa) comparing our results with other author's data.

to our PBEsol ones. On the other hand, since Karki uses the LDA approximation is normal that its results were more similar to our LDA results (except for C_{33}, which is more similar to PBEsol and C_{66}, smaller than any of ours). The results of Verma et al. vary between our LDA and PBEsol results. Finally, it is worth noting that Fouret et al. results are very similar to our PBEsol ones. Again we can see that the PBEsol approximation is the one that gets closer results to the experiments.

The values obtained for the bulk modulus using the values of the elastic constants in Tab.5 (Eq.16,17) are: $B_V = 70.00$, 51.981 and 62.161 GPa and $B_R = 69.616$, 51.699 and 61.562 GPa, respectively for the LDA, PBE and PBEsol approximations. Comparing with the values shown in Tab.1 we see that they are in good agreement. They are also quite similar to the values obtained with the linear compressibilities. This proves the consistency and goodness of our simulations.

Applying Eqs.18,19 to calculate the linear compressibilities at zero pressure given by the elastic constants we obtain: $\kappa_a = 0.0041$, 0.0055 and 0.0043 GPa^{-1}; $\kappa_c = 0.0065$, 0.0083 and 0.0076 GPa^{-1} respectively for LDA, PBE and PBEsol. The difference between these values and the ones from Tab.4 are minimum.

The evolution of these constants with pressure for the PBEsol approximation is shown in Fig.7 (the studies for LDA and PBE where made too, but they are omitted since the results are similar for the three approximations).

We observe that the elastic constant C_{44} becomes negative at 2 GPa and suddenly turns to positive again at 3 GPa. In the LDA approximation this negative pike happens between 2.5 and 3.5 GPa and with PBE between 3 and 3.5 GPa. This behaviour is related with the fact that a pressure induced phase transition could occurs around 3 GPa and that it is the elastic constant C_{44} the one that is involved, as noticed for Derollez et al. [52] and by Klotz et al. [53] with neutron scattering. We will comment later on this transition. This transition has been observed by other authors previously [41],[42],[54], but without specifying what it was due to. One thing that was known is that this pressure of the first transition in the $AgGaX_2$ chalcopyrite ($X = S, Se, Te$) decreases with the size of the anion [41]. The other features observed in Fig.7 (values of the other constants, the crosses between constants and the change of tendency over 10 GPa) are almost identical in all three approximations used.

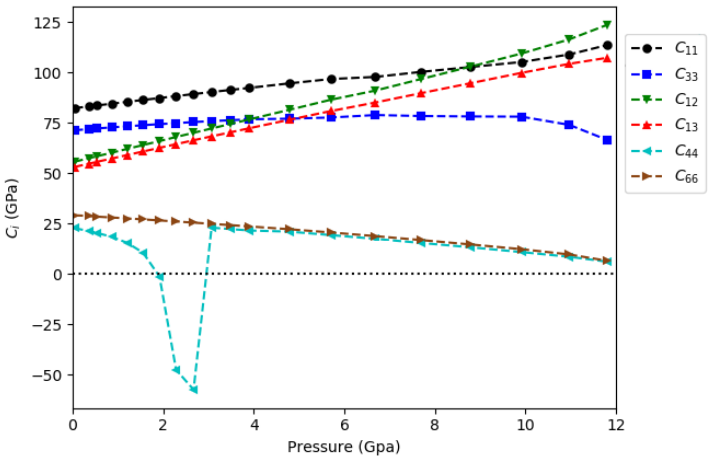

Figure 7: Evolution of the elastic constants with pressure for the PBEsol approximation.

Focusing on C_{44}, we show in Fig.8 its evolution under pressure in the three approximations.

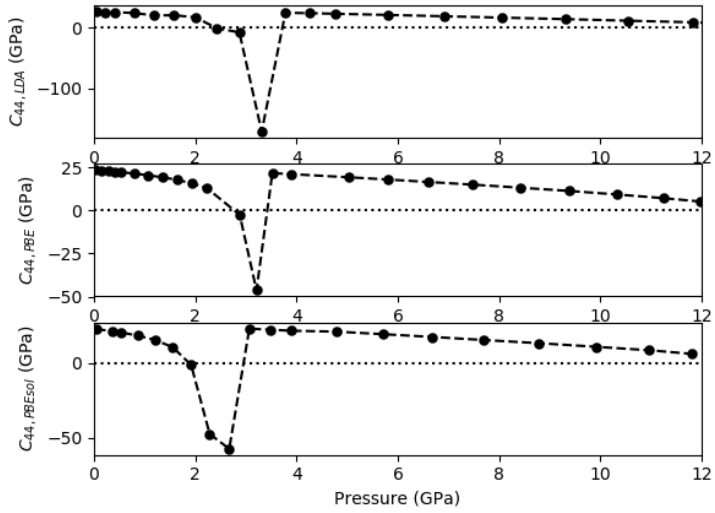

Figure 8: Evolution of the elastic constant C_{44} under pressure for the three approximations studied (LDA, PBE and PBEsol from top to bottom).

If we plot the five Born stability criteria described on Eq.15 , the results are shown in Fig.9.

On the first plot, it does not exist any instability. Referring to the second plot, we can see that the generalized stability criteria related to the elastic constant C_{44} is violated around 3 GPa. So the structure becomes mechanically unstable around this pressure, as reported by Arora et al. [41] and Klotz et al. [53] found via neutron scattering. In the third plot, the region of pressures under study does not show any instability; but, opposite to the first plot, if the tendency keeps when increasing the pressure we can estimate an instability around 14 GPa for the PBE and PBEsol approximations, and around 18 GPa for LDA. On the forth plot, the instability happens at 9 GPa for the three approximations. Finally, on the fifth plot we also

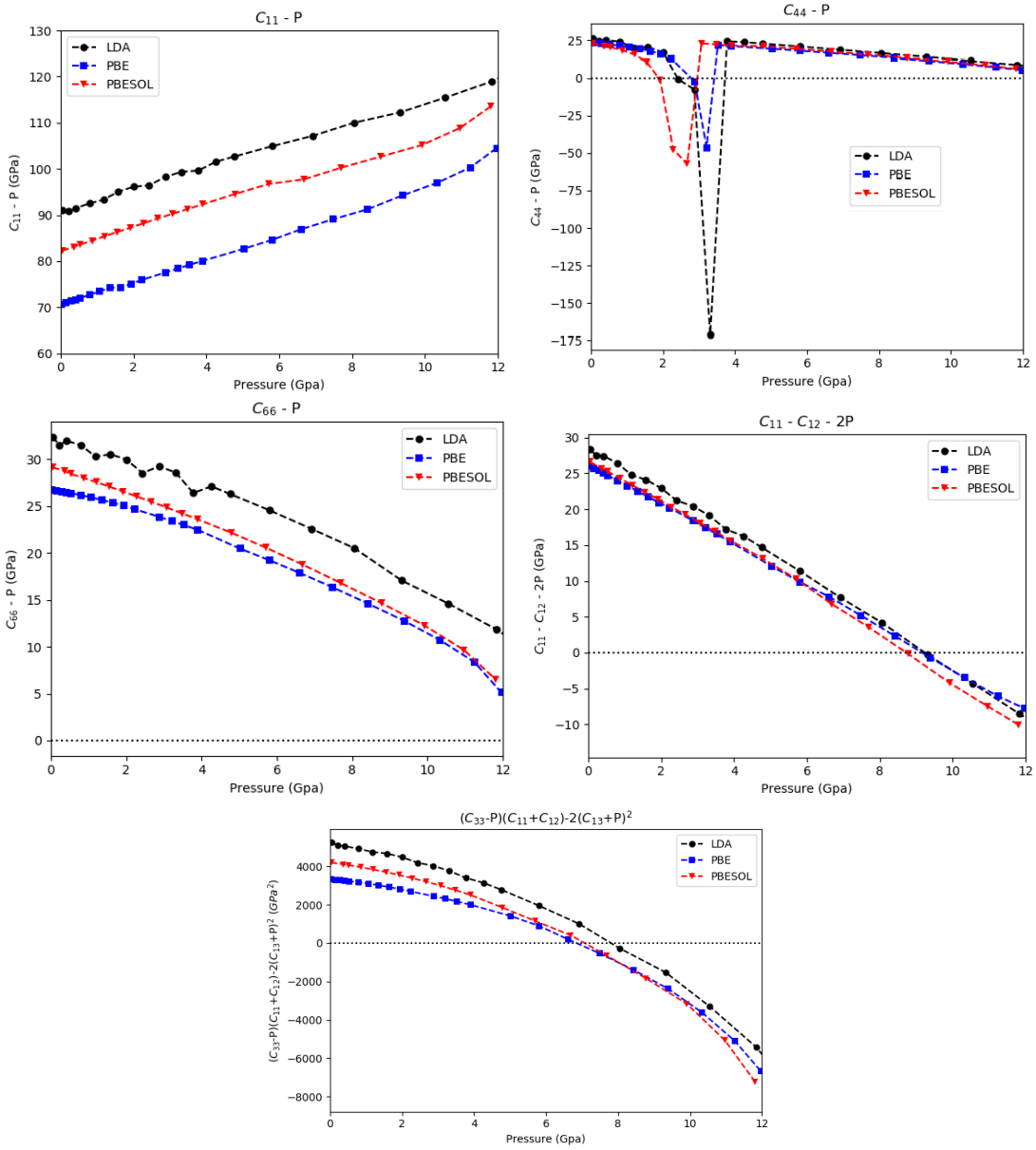

Figure 9: Representation of the five Born stability criteria.

observe an instability between 7 and 8 GPa depending on the approximation used. However, the structure under study is mechanically unstable at pressures higher than 3 GPa, as the first criteria violated is the one related with C_{44}. A transition to another phase probably occurs, but the determination of this poschalcopyrite phase is beyond the scope of the present work.

5.5 Phonons

As the primitive cell of $AgGaSe_2$ has two formula per cell (8 atoms), there exist 24 degrees of freedom which implies the existence of 21 optical modes. Group theory gives for the irreducible

representation:

$$\Gamma = 1A_1 + 2A_2 + 3B_1 + 3B_2 + 6E \tag{33}$$

where six of them are doubly degenerated (E). The A_2 modes are silent and the rest are Raman active, being the B_2 and E modes also infrared active.

Phonons were obtained, like the elastic constants, with the three approximations (LDA, PBE and PBEsol), but the following figures correspond only to the results of the PBEsol approximation and the differences with the other two approximations will be explained after the figures. The values at zero pressure, ordered from lower frequency to higher in the PBEsol approximation, are compared with data from others authors in Tab.6.

Irr. Repr.	This work			K. et al.	L. and P.	F. et al.	C. et al.
	LDA	PBE	PBEsol	[49]	[55]	[48]	[56]
E (RI)	0.792	0.833	0.699	0.78	0.60	0.81	0.81
B2 (RI)	1.727	1.574	1.615	1.80	1.85	1.76	1.74 (1.74)
B1 (R)	1.858	1.673	1.755	1.83	1.81	1.62	1.74
E (RI)	2.452	2.305	2.354	2.64	2.49	2.40	2.52 (2.52)
E (RI)	4.238	3.719	4.017	4.35	4.22	4.10	4.11 (4.14)
B1 (R)	4.805	4.411	4.615	4.68	4.76	4.68	4.80
B2 (RI)	5.023	4.323	4.730	4.77	4.75	4.95	4.65 (4.83)
A2	5.086	4.402	4.803	4.91	4.73	4.68	-
E (RI)	5.331	4.491	5.004	5.01	5.03	4.80	4.86 (4.95)
A1 (R)	5.436	4.872	5.217	5.46	5.39	-	5.43
A2	6.046	5.598	5.895	6.45	6.15	6.25	-
B1 (R)	7.261	6.634	7.001	7.35	7.17	7.10	7.58
E (RI)	7.271	6.663	7.041	7.55	7.39	7.10	7.64
B2 (RI)	7.362	6.705	7.098	7.64	7.39	8.20	7.55 (8.24)
E (RI)	7.350	6.770	7.119	7.61	7.57	7.60	7.52 (8.30)

Table 6: Irreducible representation and frequencies (THz) of the phonons at 0 GPa. In the first column, in brackets, Raman (R), infrared (I) or both (RI) active are indicated. In the last column, in brackets, the frequencies of the experimental LO modes.

From the data of Tab.6, both Karki et al. [49] and Lazewski and Parlinski [55] use *Ab Initio* methods with the LDA approximation. Fouret et al. [48] and Camassel et al. [56] data correspond to experimental results (obtained by neutron scattering and by Raman scattering respectively). Due to this, the values of Karki and Lazewski are more similar to our LDA results; however, there are some modes whose frequency is closer to our PBEsol results. Again, the experimental values of Fouret and Camassel vary between our results for the LDA and the PBEsol approximations. There are a few things that worth noting on these results: using Raman scattering allows one to distinguish the splitting LO-TO, but it do not show the silent modes. The PBE approximation gives results of smaller energy for all the modes, except from the acoustic mode, whose value is the biggest of the three. In this work we do not consider the effects of the electric field due to charges transfer between atoms. Therefore, the LO-TO splittings have not been calculated. In table 5 we show only the TO modes They compare quite

well with the experimental results.

We have also studied the behaviour of the phonons at the Γ-point with pressure using the primitive cell till a pressure of 12 GPa.

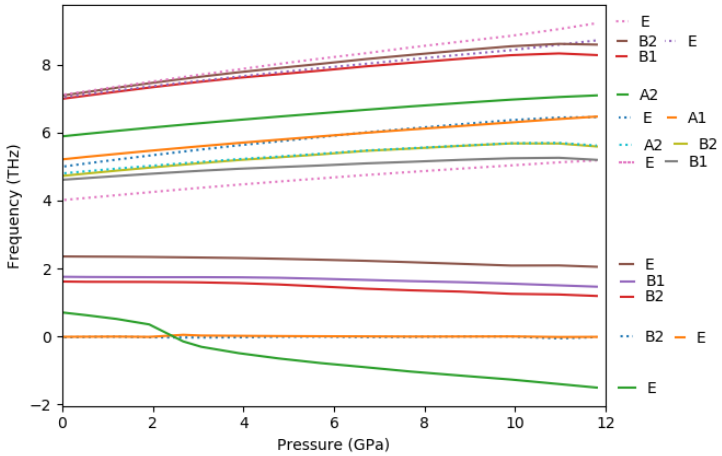

Figure 10: Pressure evolution of the $AgGaSe_2$ phonons for the PBEsol approximation.

It can be seen in Fig.10 that phonons can be grouped in different energy bands. First, with almost identical energy at zero pressure, we have 4 modes in the zone of high energy ($1B_1 + 1B_2 + 2E$) that slowly separate from each other when the pressure increases. In the intermediate region, we have 7 modes ($1A_1 + 2A_2 + 1B_1 + 1B_2 + 2E$) where one of the A_2 modes is a bit more energetic than the others in all the range under study and the other modes intersect each other with increasing pressure. Finally, in the lower energy region, there are 4 modes ($1B_1 + 1B_2 + 2E$) which, opposite to the other modes, decrease in frequency increasing with pressure. There also are three acoustic modes ($B_2 + E$) whose frequency is always very close to zero.

We see that the most important feature in Fig.10 is that one of the phonons (with irreducible representation E) suddenly becomes negative around 2.5 GPa. Therefore, this indicates the chalcopyrite structure of $AgGaSe_2$ is dynamically unstable at pressure higher than approximately 2 GPa. This also happens for the LDA and PBE approximations at 3.5 GPa in both of them. This fact was also observed by Klotz et al. [53] experimentally on neutron scattering. This softening of the E mode is related with the behaviour of the elastic constant C_{44}, which becomes negative at the same pressure. The rest of aspects (tendency of the curves and crosses between phonons) happens approximately at the same frequencies for the other two approximations. Just to comment, the frequencies given by the LDA approximation are a bit higher that the ones given the PBEsol and that with the PBE, it happens the opposite, they are a bit smaller, but the difference does not overcome 0.5 THz approximately.

Using a supercell 2x2x2 we have calculated the phonon dispersion curves inside the first Brillouin zone till a pressure of 3 GPa. The path followed has been: Γ-X-P-N-Γ-M (Fig.11). This path has been chosen following [57],[58]. We have also obtained the total density of states (TDOS) and partial density of states (PDOS). These calculation were made only for the PBEsol

approximation due to the great time cost of the process.

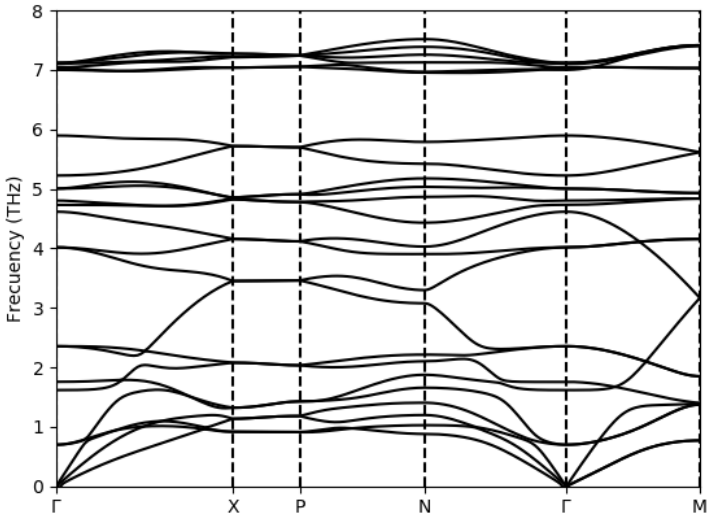

Figure 11: Phonon dispersion curves inside the first Brillouin zone at 0 GPa for the PBEsol approximation.

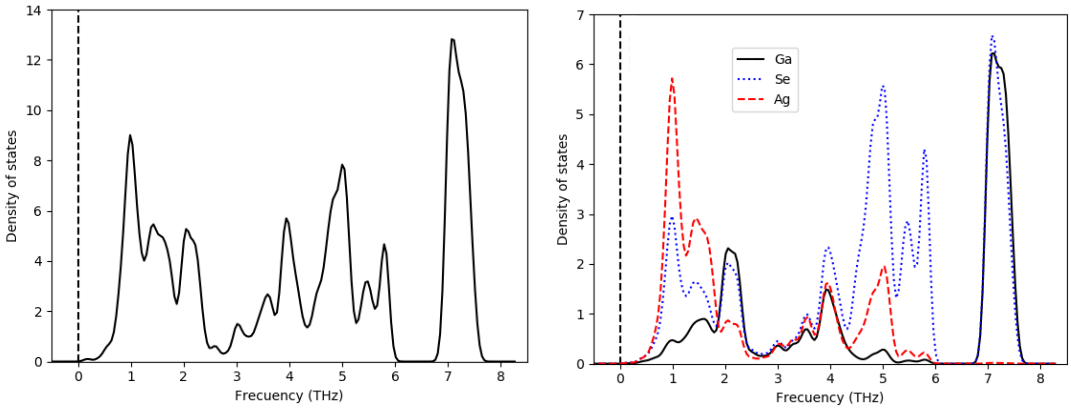

Figure 12: TDOS (left) and PDOS (right) at 0 GPa for the PBEsol approximation.

In this work we do not consider the effects of the electric field due to charges transfer between atoms. Therefore, the LO-TO splitting have not been calculated, however as shown by Lazewski and Parlinski [46], this splitting is very small. There are some differences between this work and our PDOS at 0 GPa: first, the high and intermediate bands of modes have greater frequencies in their work and, while the higher band at the Γ-point which they obtain is more splitted than ours, their intermediate band is more compact; and second, in our work there exist a gap without modes (that can be seen in Fig.12 above 6 THz) which does not appear in their work. However, these differences are smaller when we compare with a posterior work of the same authors [55]. In that work we observe that the gap appears and that the frequencies are smaller and very similar to ours (only the higher band is still more energetic, but it can be due to the LDA approximation they use that continuously give bigger results that the PBEsol one).

The only experimental data found on the literature referring to phonon dispersion curves are from Fouret et al. [48]. Although, they also obtain higher frequencies for the top band, our results are in good agreement with the experimental ones. It is known that at higher pressures, experimental and theoretical data differ more, since the difference between then is approximately 5 %.

Looking at Fig.12, we see that the contribution of the Ag-atoms to the higher frequency band is null, due to its higher mass, and that the contribution of the Ga and Se atoms is similar. In the lower frequency band, contrarily, the Ag-atoms are the ones who contribute the most to this band. In the intermediate band, there exist a transition from the low range, where all the atoms contribute the same, from the high range where the Se-atoms dominate.

The calculation of the dispersion curves inside the first Brillouin zone have also been done at a pressure of 3 GPa with the PBEsol approximation (Fig.13). At this pressure, both the C_{44} elastic constant (Fig.9) and the E-mode phonon (Fig.10) show that the crystal structure is unstable and $AgGaSe_2$ should have suffer a phase transformation according to [41],[42],[52],[53],[54].

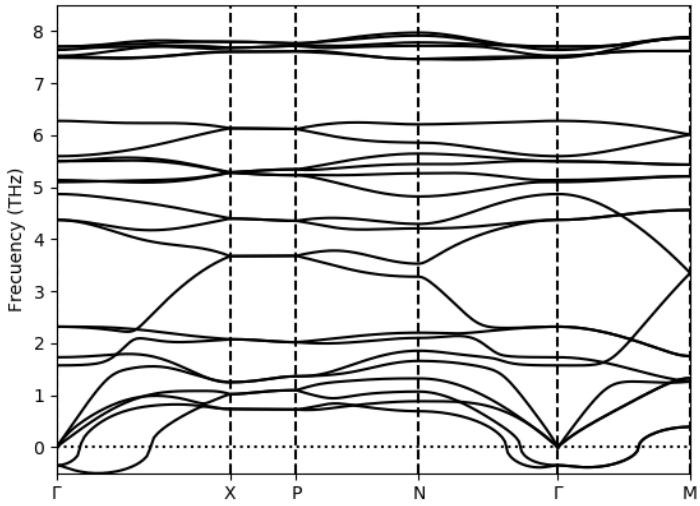

Figure 13: Phonon dispersion curves inside the first Brillouin zone at 3 GPa.

The first difference easily observable between the dispersion curves at 0 and 3 GPa is that one of the modes is negative at the Γ-point (See Fig.13). This may be due to two things: the structure is unstable or numerical errors. We can discard the numerical error because if this were the cause, and the 2x2x2 supercell were not big enough to certainly obtain the dispersion curves, this problem would have appeared in the dispersion curve at 0 GPa too; but here this problem does not exist. So we can attribute these imaginary frequencies to the fact that the structure is indeed dynamically unstable. Otherwise, the rest of the dispersion curves are very similar, with the only difference that the frequencies of the intermediate and high energy bands are a bit bigger at 3 GPa than at 0 GPa. However, this is completely normal since the modes increase their frequency with pressure, as shown in Fig.10. The frequencies of the low energy band should be smaller at 3 GPa, but this difference is more difficult to appreciate it, the slope

of the change of frequency with pressure for this phonons in Fig.10 is lower for this band than for the intermediate and high energy ones.

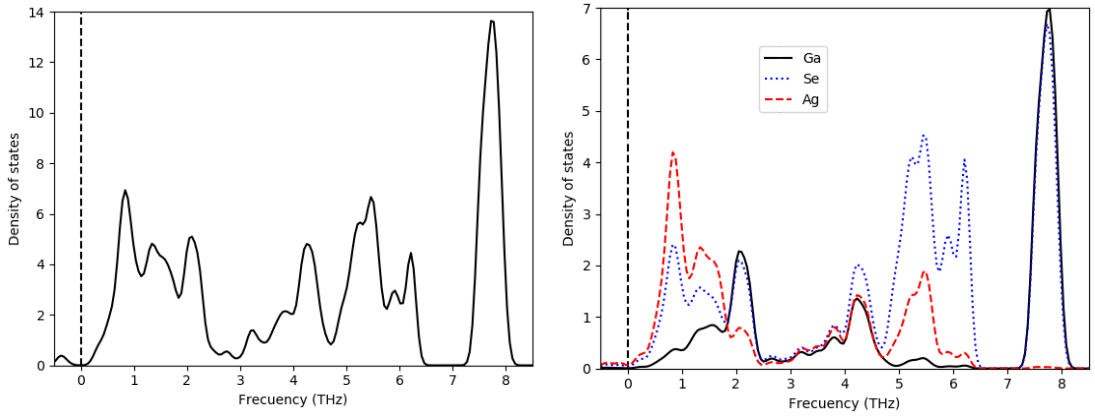

Figure 14: Total phonon density of states (left) and partial phonon density of states (right) at 3 GPa.

Studying the phonon density of states at 3 Ga in Fig.14 we see that the differences with the density of states at 0 GPa (Fig.12) are tiny. The contributions of the different atoms is exactly the same, but worth noting that at 3 GPa, the densities of the low and intermediate bands are smaller and for the high energy band is higher. We can explain this facts for three reasons: the low band "loses" one mode, which now has negative frequency, which decreases the density of states; both the low and intermediate bands are a bit wider at 3 GPa and thus the frequency at a determined frequency is smaller; the opposite happens with the high energy band, which is narrower at 3 GPa and thus the states are more concentrate.

6 Conclusion

We have seen the great importance of the *Ab Initio* methods to obtain theoretically the diverse properties of a material. Using elaborated and well tested approximations, these kind of methods allow to simulate the experimental results, which in some cases are complicated to obtain, with great accuracy. The material under study ($AgGaSe_2$) has shown its utility in many possible applications thanks to the unique characteristics that provides the fact of having a chalcopyrite structure. We have made a complete study of the structural, elastic and vibrational properties under pressure, observing the pressures at which the phase transitions happen and what mechanisms are involved.

Of the three approximations used (LDA, PBE and PBEsol), this last one has proven to give results closer to the experimental values for the volume at zero pressure and for the structural parameters of the lattice (Tabs.1,2). We have seen that the LDA approximations leads to an underestimation of the lattice parameters and thus to an overestimation of the bulk modulus. The first derivative of the bulk modulus (B_0') has similar values with the three methods.

The linear compressibilities show that the c-axis is more compressible than the a-axis

(Fig.5). The values obtained for the bulk modulus using the linear compressibilities agree with the ones obtained by the adjustment of the equation of state. These also happens with the elastic constants, whose value for the bulk modulus and for the linear compressibilities are almost exactly to the ones previously obtained. We have studied the evolution of the internal parameter u fitting to a third order polynomial (Fig.6) obtaining the coefficients shown in Tab.3.

The values at zero pressure of the experimental elastic constants are between our LDA and PBEsol values (Tab.5). We have observed that it is the C_{44}-constant which is involved in the phase transition around 2.5 GPa (Fig.8). The violation of the generalized Born stability criteria for the elastic constant C_{44} indicates that the chalcopyrite structure of $AgGaSe_2$ is dynamically unstable at higher pressures.

Finally, we have obtained the frequencies of the phonons that characterise the vibrations of the crystal structure and we have compared them, with great agreement, with other available data (Tab.6). The evolution of the frequencies of the phonons at the Γ-point has shown that one of the E-modes becomes imaginary around 2.5 GPa (Fig.10) indicating that the chalcopyrite structure of $AgGaSe_2$, apart from mechanically, is also dynamically unstable. The dispersion relation and the total and partial density of states inside the first Brillouin zone were also obtained and the contribution of each atom is discussed at 0 and 3 GPa (Figs.11-14) and we compare the phonon dispersion, TDOS and PDOS for an stable and an unstable case.

References

[1] Georg Kresse and Jürgen Furthmüller. "Efficient iterative schemes for ab initio total-energy calculations using a plane-wave basis set". In: *Physical review B* 54.16 (1996), p. 11169.

[2] John P Perdew et al. "Restoring the density-gradient expansion for exchange in solids and surfaces". In: *Physical review letters* 100.13 (2008), p. 136406.

[3] Atsushi Togo and Isao Tanaka. "First principles phonon calculations in materials science". In: *Scripta Materialia* 108 (2015), pp. 1–5.

[4] L Artus et al. "Lattice dynamics of AgGaSe 2. II. Theoretical aspects". In: *Physical Review B* 41.9 (1990), p. 5727.

[5] JE Jaffe and Alex Zunger. "Theory of the band-gap anomaly in AB C 2 chalcopyrite semiconductors". In: *Physical Review B* 29.4 (1984), p. 1882.

[6] L Artus and Y Bertrand. "Anomalous temperature dependence of fundamental gap of AgGaS2 and AgGaSe2 chalcopyrite compounds". In: *Solid state communications* 61.11 (1987), pp. 733–736.

[7] Peter G Schunemann, Scott D Setzler, and Thomas M Pollak. "Phase-matched crystal growth of AgGaSe2 and AgGa1- xInxSe2". In: *Journal of Crystal Growth* 211.1-4 (2000), pp. 257–264.

[8] Y Satyanarayana Murthy et al. "Characterization of p-AgGaSe2/n-CdS thin film heterojunction". In: *Materials Letters* 10.11-12 (1991), pp. 504–508.

[9] Ingrid Repins et al. "19· 9%-efficient ZnO/CdS/CuInGaSe2 solar cell with 81· 2% fill factor". In: *Progress in Photovoltaics: Research and applications* 16.3 (2008), pp. 235–239.

[10] C Merschjann et al. "AgGaSe2 thin films grown by chemical close-spaced vapor transport for photovoltaic applications: structural, compositional and optical properties". In: *Journal of Physics: Condensed Matter* 24.17 (2012), p. 175801.

[11] Timothy J Coutts et al. "Critical issues in the design of polycrystalline, thin-film tandem solar cells". In: *Progress in Photovoltaics: Research and Applications* 11.6 (2003), pp. 359–375.

[12] Utpal N Roy et al. "Crystal growth, characterization, and fabrication of AgGaSe 2 crystals as novel material for room-temperature radiation detectors". In: *Hard X-Ray and Gamma-Ray Detector Physics VI*. Vol. 5540. International Society for Optics and Photonics. 2004, pp. 177–181.

[13] RC Eckardt et al. "Broadly tunable infrared parametric oscillator using AgGaSe2". In: *Applied physics letters* 49.11 (1986), pp. 608–610.

[14] PG Schunemann, KL Schepler, and PA Budni. "Nonlinear frequency conversion performance of AgGaSe 2, ZnGeP 2, and CdGeAs 2". In: *Mrs Bulletin* 23.7 (1998), pp. 45–49.

[15] Sergey N Rashkeev and Walter RL Lambrecht. "Second-harmonic generation of I-III-VI 2 chalcopyrite semiconductors: Effects of chemical substitutions". In: *Physical Review B* 63.16 (2001), p. 165212.

[16] RC Eckardt et al. "Efficient second harmonic generation of 10-μm radiation in AgGaSe2". In: *Applied physics letters* 47.8 (1985), pp. 786–788.

[17] K Stoll, J-J Zondy, and O Acef. "Fourth-harmonic generation of a continuous-wave CO 2 laser by use of an AgGaSe 2/ZnGeP 2 doubly resonant device". In: *Optics letters* 22.17 (1997), pp. 1302–1304.

[18] Eiko Takaoka and Kiyoshi Kato. "90° phase-matched third-harmonic generation of CO 2 laser frequencies in AgGa 1–x In x Se 2". In: *Optics letters* 24.13 (1999), pp. 902–904.

[19] Yunlong Cui et al. "Raman spectroscopy study of AgGaSe2, AgGa0. 9In0. 1Se2, and AgGa0. 8In0. 2Se2 crystals". In: *Solid State Communications* 150.35-36 (2010), pp. 1686–1689.

[20] GC Bhar et al. "Efficient generation of mid-infrared radiation in an AgGaxIn 1- xSe 2 crystal". In: *Optics letters* 20.20 (1995), pp. 2057–2059.

[21] Jose Manuel Recio, Jose Manuel Menendez, and Alberto Otero De la Roza. *An introduction to high-pressure science and technology*. CRC Press, 2016.

[22] Pierre Hohenberg and Walter Kohn. "Inhomogeneous electron gas". In: *Physical review* 136.3B (1964), B864.

[23] Walter Kohn and Lu Jeu Sham. "Self-consistent equations including exchange and correlation effects". In: *Physical review* 140.4A (1965), A1133.

[24] Wikipedia. *Pseudopotential*. URL: https://en.wikipedia.org/wiki/Pseudopotential (visited on 03/07/2019).

[25] Hendrik J Monkhorst and James D Pack. "Special points for Brillouin-zone integrations". In: *Physical review B* 13.12 (1976), p. 5188.

[26] John Frederick Nye et al. *Physical properties of crystals: their representation by tensors and matrices*. Oxford university press, 1985.

[27] Max Born. "On the stability of crystal lattices. I". In: *Mathematical Proceedings of the Cambridge Philosophical Society*. Vol. 36. 2. Cambridge University Press. 1940, pp. 160–172.

[28] Félix Mouhat and François-Xavier Coudert. "Necessary and sufficient elastic stability conditions in various crystal systems". In: *Physical Review B* 90.22 (2014), p. 224104.

[29] Woldemar Voigt. *Lehrbuch der kristallphysik*. Vol. 962. Teubner Leipzig, 1928.

[30] A Reuss. "Berechnung der fließgrenze von mischkristallen auf grund der plastizitätsbedingung für einkristalle." In: *ZAMM-Journal of Applied Mathematics and Mechanics/Zeitschrift für Angewandte Mathematik und Mechanik* 9.1 (1929), pp. 49–58.

[31] B Mayer et al. "Ab-initio calculation of the elastic constants and thermal expansion coefficients of Laves phases". In: *Intermetallics* 11.1 (2003), pp. 23–32.

[32] Stefano Baroni et al. "Phonons and related crystal properties from density-functional perturbation theory". In: *Reviews of Modern Physics* 73.2 (2001), p. 515.

[33] Georg Kresse and D Joubert. "From ultrasoft pseudopotentials to the projector augmented-wave method". In: *Physical Review B* 59.3 (1999), p. 1758.

[34] Yvon Le Page and Paul Saxe. "Symmetry-general least-squares extraction of elastic data for strained materials from ab initio calculations of stress". In: *Physical Review B* 65.10 (2002), p. 104104.

[35] Francis Dominic Murnaghan. "Finite deformations of an elastic solid". In: *American Journal of Mathematics* 59.2 (1937), pp. 235–260.

[36] R Asokamani et al. "Electronic structure calculations and physical properties of ABX2 (A= Cu, Ag; B= Ga, In; X= S, Se, Te) ternary chalcopyrite systems". In: *physica status solidi (b)* 213.2 (1999), pp. 349–363.

[37] A Chahed et al. "First-principles calculations of the structural, electronic and optical properties of AgGaS2 and AgGaSe2". In: *Physica B: Condensed Matter* 367.1-4 (2005), pp. 142–151.

[38] Shiyou Chen, XG Gong, and Su-Huai Wei. "Band-structure anomalies of the chalcopyrite semiconductors CuGa X 2 versus AgGa X 2 (X= S and Se) and their alloys". In: *Physical Review B* 75.20 (2007), p. 205209.

[39] Tarik Ouahrani et al. "Elastic properties and bonding of the AgGaSe2 chalcopyrite". In: *Physica B: Condensed Matter* 405.17 (2010), pp. 3658–3664.

[40] NS Orlova, OE Andreeva, and IV Bodnar. "Pressure Effects on the Structural and Elastic Properties of AgGaS2–AgGaSe2Crystals: An X-ray Diffraction Study". In: *Inorganic materials* 37.6 (2001), pp. 548–555.

[41] Akhilesh K Arora, T Sakuntala, and L Artus. "Raman spectroscopic study of high pressure phase transitions in AgGaSe2". In: *Journal of Physics and Chemistry of Solids* 54.3 (1993), pp. 381–385.

[42] T Tinoco et al. "Equation of state and phase transitions in AgGaS2 and AgGaSe2". In: *Journal of Physics and Chemistry of Solids* 56.3-4 (1995), pp. 481–484.

[43] GW Iseler. "Thermal expansion and seeded Bridgman growth of AgGaSe2". In: *Journal of Crystal Growth* 41.1 (1977), pp. 146–150.

[44] Peter G Schunemann, Scott D Setzler, and Thomas M Pollak. "Phase-matched crystal growth of AgGaSe2 and AgGa1- xInxSe2". In: *Journal of Crystal Growth* 211.1-4 (2000), pp. 257–264.

[45] Sheetal Sharma, AS Verma, and VK Jindal. "Ab initio studies of structural, electronic, optical, elastic and thermal properties of silver gallium dichalcogenides (AgGaX2: X= S, Se, Te)". In: *Materials Research Bulletin* 53 (2014), pp. 218–233.

[46] J Łażewski and K Parlinski. "Phonons in chalcopyrite crystals within the force field approach". In: *physica status solidi (b)* 218.2 (2000), pp. 411–416.

[47] J Łażewski et al. "Ab initio elasticity of chalcopyrites". In: *Journal of applied physics* 93.7 (2003), pp. 3789–3795.

[48] R Fouret et al. "Phonons in silver gallium diselenide". In: *Journal of Physics: Condensed Matter* 9.31 (1997), p. 6579.

[49] BB Karki, GJ Ackland, and J Crain. "Elastic instabilities in crystals from ab initio stress-strain relations". In: *Journal of Physics: Condensed Matter* 9.41 (1997), p. 8579.

[50] AS Verma et al. "Elastic properties of chalcopyrite structured solids". In: *Materials Chemistry and Physics* 132.2-3 (2012), pp. 416–420.

[51] H Neumann. "Lattice dynamics and related properties of AIBIII and AIIBIV compounds, I. Elastic constants". In: *journal of Experimental and Industrial Crystallography* 39.11 (2004), pp. 939–958.

[52] P Derollez et al. "Pressure Dependence of Acoustic Modes in AgGaSe2". In: *high pressure research* 22.2 (2002), pp. 283–286.

[53] S Klotz et al. "Anomalous pressure dependence of acoustic phonons of AgGaSe2 investigated by inelastic neutron scattering to 4.3 GPa". In: *physica status solidi (b)* 235.2 (2003), pp. 331–336.

[54] Y Mori et al. "High pressure structural study of I-III-VI2 chalcopyrites". In: *physica status solidi (b)* 198.1 (1996), pp. 427–431.

[55] J Lazewski and K Parlinski. “First-principles calculations for phonons in AgGaX2 (X= Se, Te) chalcopyrite crystals”. In: *Journal of Physics: Condensed Matter* 11.48 (1999), p. 9673.

[56] J Camassel, L Artus, and J Pascual. “Lattice dynamics of AgGaSe 2. I. Experiment”. In: *Physical Review B* 41.9 (1990), p. 5717.

[57] Yoyo Hinuma et al. “Band structure diagram paths based on crystallography”. In: *Computational Materials Science* 128 (2017), pp. 140–184.

[58] Atsushi Togo and Isao Tanaka. “{Spglib} : a software library for crystal symmetry search”. In: *arXiv preprint arXiv:1808.01590* (2018).